15TH IEA HEAT PUMP CONFERENCE
MAY 26–29, 2026 | HOFBURG
VIENNA 2026
DECARBONISATION THROUGH INNOVATION

Analyzing releasable refrigerant charge in a residential R290 heat pump through 1D dynamic distribution modeling

Felix Hochwallner[a,*], Stephan Preisinger[b], Adam Buruzs[a], Heinz Moisi[b], Christoph Reichl[a]

[a] AIT Austrian Institute of Technology, Center for Energy, Giefinggasse 2, Vienna 1210, Austria
[b] OCHSNER Wärmepumpen GmbH, Research & Development, Dieselstraße 6, Mauer bei Amstetten 3362, Austria

Abstract

Despite the ongoing energy transition, gas boilers remain widely used in European cities, especially in large multi-family houses. Heat pumps offer a sustainable alternative, but the tightening of the F-Gas Regulation and the shift to natural refrigerants, such as propane (R290), pose challenges due to flammability and the need for advanced safety concepts.

The Austrian national project WISE is developing a compact indoor heat pump concept with a refrigerant charge above 150 g, while limiting the releasable charge to below 150g in accordance with IEC 60335-2-40. To support this design, a physics-based one-dimensional (1D) model was developed in Dymola/Modelica to predict the component-wise refrigerant distribution and to improve charge estimation accuracy beyond conventional homogeneous equilibrium models (HEM). The model replaces the HEM assumption with separated-flow formulations based on established slip-ratio correlations (Zivi, Premoli, Ali–Sadatomi–Kawaji) and accounts for refrigerant solubility in compressor oil using experimental data for RENISO PAG 100 from Fuchs Lubricants. Separated-flow modeling and oil solubility together increase the predicted refrigerant charge significantly compared to HEM, emphasizing the importance of these effects for safety-critical design. The resulting component-wise charge breakdown provides a foundation for assessing releasable charge and optimizing component volumes.

Simulations across representative operating points, B0/W35 @ 120 Hz (nominal heating), B−15/W70 @ 80 Hz (domestic hot water generation), and B5/W24 @ 20 Hz (low-load heating), were conducted to determine the maximum admissible system charge while maintaining less than 150 g in each component. The results show that the condenser consistently stores the largest portion of the total charge, making it the most critical component for compliance with the releasable-charge limit. Using the conservative Premoli correlation, the maximum permissible total system charge was found to be approximately 269 g for the analyzed heat pump, limited by the domestic-hot-water operating point (B−15/W70 @ 80 Hz).

Keywords: R290; propane; charge; releasable charge; distibution modeling

1. Introduction

Space and water heating account for a major share of building energy demand, while natural gas still dominates the European heating mix. To decarbonize this sector, policies increasingly promote the replacement of gas boilers with heat pumps [1]. At the same time, the new F-Gas Regulation (EU 2024/573) [2] and international agreements such as the Kigali Amendment to the Montreal Protocol [3] are tightening restrictions on refrigerants with high global warming potential (GWP). As a result, natural refrigerants such as propane

* Corresponding author. Tel.: +43 664 8157941
E-mail address: felix.hochwallner@ait.ac.at

15th IEA Heat Pump Conference 2026 - HDU3.2 - https://doi.org/10.23697/jxzw-k236

(R290) are gaining importance due to their excellent thermodynamic performance and very low GWP (0.02 [2]). However, their flammability poses safety challenges for systems installed in occupied indoor spaces.

To address these risks, safety standards such as EN 378-1:2021 [4] and IEC 60335-2-40 [5] define strict design and installation criteria for systems using flammable refrigerants. These standards limit the amount of refrigerant that may be released into an occupied space during a leak. While previous editions set limits on the total charge, the 7th edition of IEC 60335-2-40 defines limits based on the maximum releasable charge. This shift allows systems to contain more than 150 g of R290, provided that the potentially releasable mass remains below the threshold. Consequently, the focus of safety design has moved from total filling quantity to accurate prediction of refrigerant distribution among components under all operating conditions.

Conventional homogeneous equilibrium models (HEM) tend to underestimate the refrigerant mass in two-phase regions, especially in heat exchangers, leading to overly optimistic safety assessments [6], [7]. Furthermore, a significant portion of the total charge can be dissolved in compressor oil. Measurements on a brine-to-water R290 heat pump reported up to 41.5 % of the charge stored in the compressor, predominantly in the oil phase [8]. These findings highlight the necessity of detailed, component-resolved charge modeling that captures both phase slip and oil solubility effects.

Within the Austrian national project WISE, we therefore developed a physics-based one-dimensional (1D) simulation model in Dymola/Modelica using the TIL Suite. The model replaces the HEM assumption with separated-flow (slip-ratio) correlations and integrates propane solubility in compressor oil to enable realistic estimation of the total and component-wise refrigerant charge. The resulting charge distributions are used to verify compliance with the 150 g releasable-charge limit and to identify critical operating conditions. These insights form the basis for future coupling with 3D CFD leakage simulations and for design optimization of safe, compact R290 heat pumps intended for indoor residential installation.

2. Methods

A one-dimensional, component-based model of the propane heat pump was developed in Dymola/Modelica using the TIL Suite from TLK-Thermo [9], which provides validated libraries for thermodynamic system simulation and property calculation. The model comprises all major circuit elements - compressor, evaporator, condenser, tubes and auxiliary components like filter dryer, and sight glass - each represented by standardized or extended TIL components. The model explicitly includes the internal volumes of all components according to the real system layout, and a rotary compressor and brazed plate heat exchangers are used. The connecting lines were modeled as adiabatic, simulations were conducted under steady-state conditions, and refrigerant properties were obtained from TILMedia, which employs high-accuracy real-fluid equations of state for propane using splines for fast evaluation. To improve the accuracy of refrigerant charge estimation, the refrigerant solubility in compressor oil was implemented to capture the share of propane dissolved in the lubricant and its contribution to the total refrigerant charge. The standard homogeneous equilibrium model assumption of the TIL heat-exchanger model was replaced by a separated-flow model that accounts for slip between the vapor and liquid phases.

2.1. Compressor Oil Solubility

Refrigerant solubility in compressor oil can significantly influence the total charge distribution, particularly for highly soluble systems such as propane in polyalkylene glycol (PAG) oils. To account for this effect, the solubility of R290 in the lubricant was implemented using data from Fuchs Lubricants for RENISO PAG 100 [10]. The publicly available vapor-pressure chart of the oil–propane mixture was digitized, which provides the vapor pressure as a function of temperature in the range of 0–80 °C for several propane concentrations (1–20 wt %) including pure propane. The data were linearly interpolated in temperature and pressure to determine the corresponding equilibrium concentration of dissolved propane in oil at the local compressor discharge conditions. Figure 1 illustrates the digitized vapor-pressure data for R290 - RENISO PAG100 mixtures from Fuchs Lubricants, showing the equilibrium vapor pressure as a function of temperature and propane mass fraction. This dataset forms the basis for the interpolation routine used to evaluate oil solubility in the model.

In the model, all compressor oil is assumed to be located on the discharge (hot-gas) side, as a rotary compressor is used, and the total oil mass is fixed at 300 g based on manufacturer specifications. The calculated solubility is used solely for refrigerant charge accounting and does not influence the thermodynamic performance, heat transfer, or pressure-drop calculations of the system. This approach provides a realistic estimate of the refrigerant fraction stored in the compressor oil, thereby ensuring more accurate component-wise charge prediction, while maintaining numerical stability of the steady-state simulation.

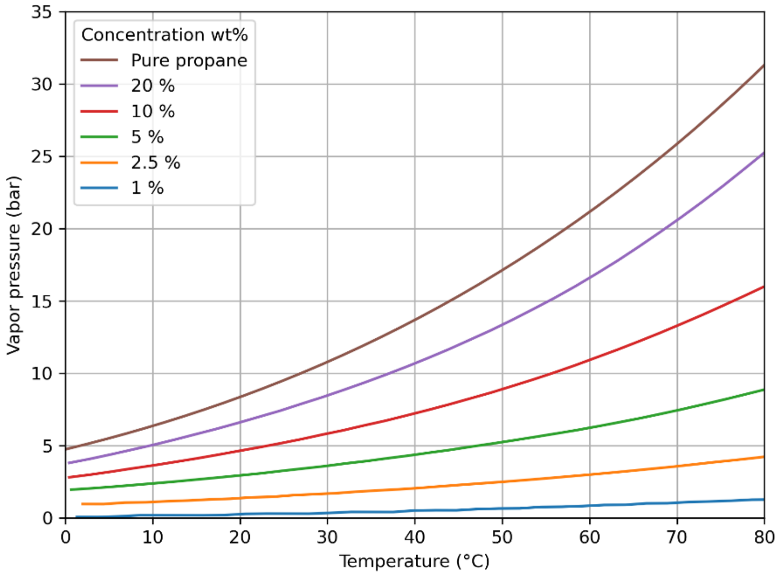

Figure 1: Digitized vapor-pressure data of R290 - RENISO PAG100 mixtures used to estimate propane solubility in compressor oil. Data source: Fuchs Lubricants [17].

2.2. Separated-flow model

In the default configuration of the TIL library, two-phase flow in heat exchangers is modeled using the homogeneous equilibrium model. In this approach, the liquid and vapor phases are assumed to move at the same velocity and remain in thermodynamic equilibrium. While this assumption simplifies the governing equations, it tends to underestimate the refrigerant charge in heat exchangers, particularly in the two-phase regions where the vapor travels faster than the liquid phase. The resulting overprediction of void fraction leads to lower predicted densities and thus to an underestimation of the total fill mass.

To improve the prediction accuracy, a separated-flow model was implemented. This approach assumes different velocities for the vapor and liquid phases, linked through the slip ratio s, defined as the ratio of the vapor velocity v_{vap} to the liquid velocity v_{liq}:

$$s = \frac{v_{vap}}{v_{liq}} \tag{1}$$

The void fraction α represents the ratio of the cross-sectional area occupied by the vapor phase to the total flow area and is related to the slip ratio s, vapor quality x, and densities ρ_{vap} and ρ_{liq} by:

$$\alpha = \frac{A_{vap}}{A_{tot}} = \frac{1}{1+\frac{1-x}{x} s \frac{\rho_{vap}}{\rho_{liq}}} \tag{2}$$

The total mixture density ρ_{tot} is then obtained from:

$$\rho_{tot} = \alpha\, \rho_{vap} + (1-\alpha)\, \rho_{liq} \tag{3}$$

To calculate the slip ratio, several correlations exist in the literature. Based on the detailed review by Winkler et al. (2012) [6], four representative models of increasing complexity were considered and implemented in this work: HEM, Zivi [11], Premoli [12], and Ali–Sadatomi–Kawaji [13]. Each model applies a different physical assumption to describe phase slip and void-fraction behaviour, and together the four void-fraction correlations span a broad spectrum of underlying physics and conservatism.

HEM assumes perfect phase equilibrium with no slip between liquid and vapor, typically yielding the lowest void fractions and charge predictions. Zivi's correlation introduces a momentum-based slip model with a simple analytical form, offering a robust and computationally light improvement over HEM. Premoli's correlation accounts for shear and inertia effects more explicitly and is known to predict the lowest void fractions - making it the most conservative and yielding the highest charge estimates. The Ali–Sadatomi–Kawaji (ASK) model incorporates geometric effects and is particularly suited for narrow channels. However, it should be noted that most slip-ratio correlations were originally developed for circular or rectangular tube geometries. Their applicability to brazed plate heat exchangers is therefore uncertain, since the complex, corrugated channel geometry may lead to non-uniform phase distribution. Consequently, a key question remains regarding how accurately these models can represent the true void fraction behavior in such complex geometries.

2.2.1. Homogeneous Equilibrium Model (HEM)

The simplest case assumes no slip between the phases, therefore both phases move at the same velocity:

$$s_{HEM} = 1 \tag{4}$$

The model results in the highest void fraction and the lowest predicted mixture density. HEM typically underestimates the refrigerant charge, particularly in low-mass-flux and horizontal flow conditions.

2.2.2. Zivi (1964) – Minimum entropy production model

Zivi derived the slip ratio from the principle of minimum entropy production in adiabatic two-phase flow, leading to:

$$s_{Zivi} = \left(\frac{\rho_{liq}}{\rho_{vap}}\right)^{1/3} \tag{5}$$

This physically based expression predicts moderate slip, physically consistent trends and offers a good numerical stability. According to Winkler et al. [6], it performs well for adiabatic and moderately condensing flows but tends to overpredict void fraction at high mass fluxes.

2.2.3. Premoli et al. (1970) – Empirical correlation from pressure-drop and holdup data

Premoli proposed an empirical correlation based on large datasets for refrigerants and air-water flows, using the liquid-only Reynolds Re_{LO} and Weber We_{LO} numbers:

$$Re_{LO} = \frac{G\,D_h}{\mu_{liq}},\ We_{LO} = \frac{G^2\,D_h}{\rho_{liq}\,\sigma} \tag{6}$$

with G the mass flux, D_h the hydraulic diameter, μ_{liq} the liquid dynamic viscosity, σ the surface tension. The slip ratio is then obtained by:

$$s_{Premoli} = 1 + E_1 \sqrt{\frac{1}{\frac{1-\alpha_{HEM}}{\alpha_{HEM}}+E_2} - \frac{\alpha_{HEM}}{1-\alpha_{HEM}} E_2} \tag{7}$$

with:

$$E_1 = 1.578\,Re_{LO}^{-0.19} \left(\frac{\rho_{liq}}{\rho_{vap}}\right)^{0.22},\ E_2 = 0.0273\,We_{LO}\,Re_{LO}^{-0.51} \left(\frac{\rho_{liq}}{\rho_{vap}}\right)^{-0.08} \tag{8}$$

This model accounts for inertia and surface-tension effects and generally predicts higher liquid holdup. Winkler et al. [6] identified it as one of the most conservative correlations, yielding low void fractions and therefore higher estimated refrigerant mass.

2.2.4. Ali–Sadatomi–Kawaji (1992) – Flow-pattern-based correlation

Ali, Sadatomi and Kawaji (ASK) proposed a drift-flux type correlation originally developed for narrow rectangular channels between parallel plates, based on flow visualization and mechanistic modeling. It introduces the Lockhart–Martinelli parameter X_{tt}:

$$X_{tt} = \left(\frac{1-x}{x}\right)^{0.9} \left(\frac{\rho_{vap}}{\rho_{liq}}\right)^{0.5} \left(\frac{\mu_{liq}}{\mu_{vap}}\right)^{0.1} \tag{9}$$

and a geometry constant $C_{ASK} = 20$. The void fraction is then directly computed as:

$$\alpha_{ASK} = 1 - \left(1 + \frac{C_{ASK}}{X_{tt}} + \frac{1}{X_{tt}^2}\right)^{-1/2} \tag{10}$$

The ASK model accounts for flow regime and channel confinement effects, showing improved agreement with experimental data for mini- and microchannels. Winkler et al. [6] reported that it achieves good accuracy for condensing refrigerants in compact geometries, especially at high mass flux.

2.3. Maximum system charge

Determining the maximum total system charge that is allowed ensures that no individual component exceeds the 150 g limit at representative operating points. Three representative operating points are evaluated: B0/W35 @ 120Hz for nominal heating at full power, B-15/W70 @ 80Hz for domestic hot water generation, and B5/W24 @ 20Hz for low-load heating. For each operating point k, the maximum admissible total charge $m_{tot,max,k}$ is defined as the charge at which any component reaches the charge limit of 150 g. The system-wide maximum filling $m_{tot,max}$ is therefore obtained by the operating point with the smallest value of maximum admissible total charge $m_{tot,max,k}$:

$$m_{tot,max} = \min_{k} m_{tot,max,k} \tag{11}$$

2.4. Performance evaluation

The Carnot efficiency was used as a dimensionless indicator of the thermodynamic performance of the heat pump relative to its theoretical maximum efficiency. It was calculated as the ratio between the calculated coefficient of performance (COP) and the corresponding Carnot COP, which represents an ideal reversible cycle operating between the same source and sink temperatures. The Carnot COP for heating mode is defined as:

$$COP_{Carnot} = \frac{T_H}{T_H - T_C} = \frac{T_{sink,out}}{T_{sink,out} - T_{source,in}} \tag{12}$$

Where T_H is the hot and T_C the cold temperature. For the analyzed compression heat pump cycle these correspond to the sink outlet temperature $T_{sink,out}$ and source inlet temperature $T_{source,in}$, respectively. Accordingly, the Carnot efficiency η_{carnot} is expressed as:

$$\eta_{carnot} = \frac{COP_{calculated}}{COP_{Carnot}} \tag{13}$$

This formulation enables a fair comparison between different operating points at various temperature levels, providing a normalized measure of how closely the real cycle approaches the thermodynamic limit.

3. Results and Discussion

To assess the influence of phase slip and oil solubility on the total refrigerant charge, simulations were performed for the operating condition B0/W35 @ 120 Hz using a baseline charge of 200 g R290 determined with the homogeneous equilibrium model. The objective was to quantify how different slip-ratio correlations affect the predicted charge distribution in the condenser and evaporator, and to evaluate the amount of refrigerant additionally retained in the compressor due to dissolution in the lubricating oil.

3.1. Effect of separated-flow model and compressor oil solubility

Figure 2 (a) compares the predicted refrigerant mass in the condenser and evaporator using the homogeneous equilibrium model and three slip-ratio correlations (Zivi, Premoli, and Ali–Sadatomi–Kawaji). Overall, the introduction of slip increases the predicted total charge compared to the HEM assumption. The condenser charge rises moderately by +16 % (Zivi), +32 % (Premoli), and +6 % (ASK), whereas the evaporator charge is much more sensitive, increasing by +117 %, +365 %, and +149 %, respectively. This strong asymmetry mainly originates from the lower density of the refrigerant in the evaporator, which results in a significantly lower absolute refrigerant charge. In absolute terms, the condenser charge increased from around 111 g (HEM) to approximately 147 g (Premoli), and the evaporator charge increased from around 12 g (HEM) to approximately 56 g (Premoli).

The results clearly show that the estimated charge is highly dependent on the chosen slip model, particularly for the evaporator. The Premoli correlation yields the highest charge, while Zivi gives a moderate correction and ASK the lowest. These differences highlight that even within established correlations, the predicted void fraction can vary significantly under the same operating conditions. Given that most of these correlations were developed for circular tubes, their transferability to brazed plate heat exchangers (BPHEs) is uncertain. This uncertainty should therefore be considered when interpreting model results and when calibrating against experimental charge measurements.

For the subsequent analysis, the Premoli correlation was selected, as it predicts the most conservative, that is, the highest, overall refrigerant mass among the tested models, providing a safety margin for charge estimation and design assessment.

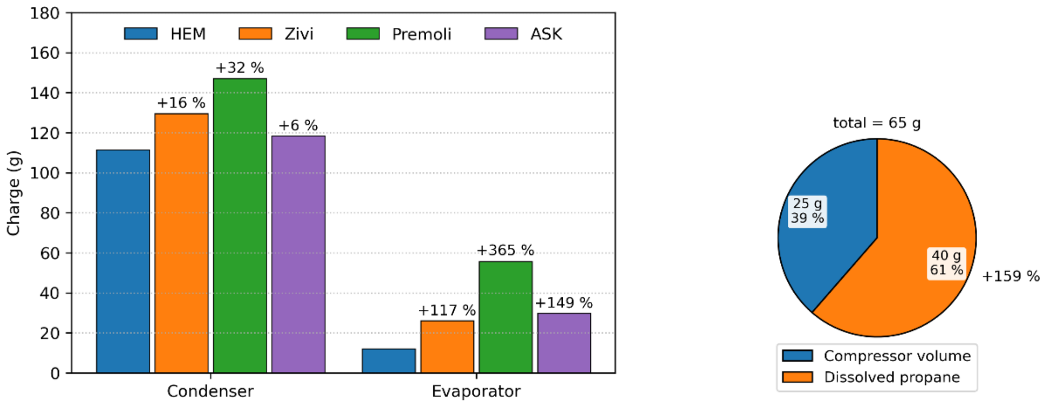

(a) Refrigerant mass in condenser and evaporator predicted using the homogeneous equilibrium model and three slip correlations (Zivi, Premoli, Ali–Sadatomi–Kawaji).

(b) Refrigerant mass in the gas volume compared to the mass dissolved in compressor oil.

Figure 2: Comparison of refrigerant charge predicted by different slip-ratio correlations and the effect of refrigerant solubility in compressor oil for operating condition B0/W35 @ 120 Hz and a total charge of 200 g (HEM).

Figure 2 (b) shows the refrigerant mass in the compressor, contained in the compressor volume and dissolved in the compressor oil. Approximately 25 g of refrigerant is contained in the compressor volume, while an additional 40 g is dissolved in the oil, corresponding to a total increase of +159 %. This confirms that oil solubility represents one large single contribution to total system charge, in agreement with recent measurements on propane systems [14]. Reducing this solubility offers a major lever for further charge reduction. This may be achieved for example by higher superheat, lower amount of oil, with oil-return optimization, or selection of low-solubility lubricants. Following this comparison, the component-wise refrigerant distribution across all system elements is analyzed to identify dominant charge holders.

3.2. Component-wise charge distribution

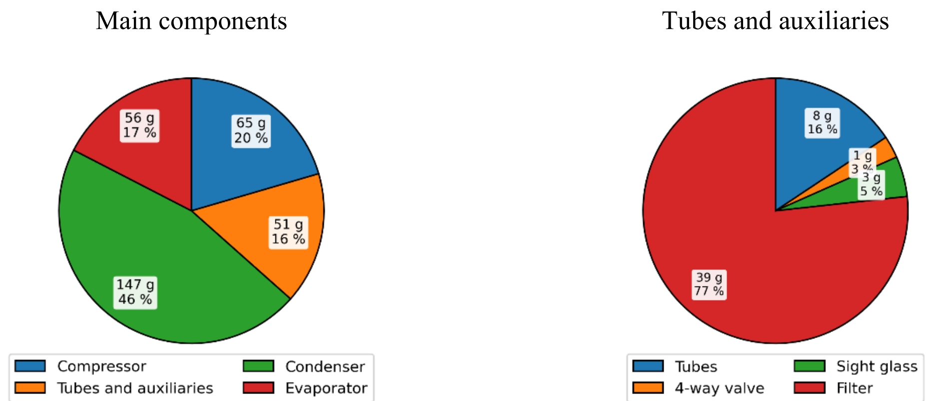

(a) Distribution of total refrigerant charge across the primary components - compressor, condenser, evaporator, tubes and auxiliary parts.

(b) Breakdown of the refrigerant charge within the tubing and auxiliary elements, including the sight glass, 4-way valve, and filter dryer.

Figure 3: Distribution of refrigerant mass among the main system components and detailed tubing and auxiliary elements of the prototype heat pump for operating condition B0/W35 @ 120 Hz and a total charge of 200 g (HEM).

Figure 3 (a) shows the distribution of the total refrigerant charge among the main components of the heat pump, compressor, condenser, evaporator, tubes and auxiliaries for the operating condition B0/W35 @ 120 Hz. The results indicate that the condenser accounts for the largest share of the total charge, while the other main components split the remaining charge into nearly equal shares. This means, that if no single component shall exceed a charge of 150 g propane, to be able to limit the amount of releasable charge to below 150 g, the condenser is the main component to consider. Figure 3 (b) provides a detailed breakdown of the refrigerant mass contained in the tubing and auxiliary components, including the sight glass, 4-way valve, and filter dryer. The results show that the filter dryer dominates this breakdown, accounting for approximately 77 % of the total mass in this group, followed by the connecting tubes (16 %), sight glass (5 %), and 4-way valve (3 %). Although these elements represent relatively small internal volumes compared to the main heat exchangers, their cumulative contribution remains non-negligible, emphasizing the importance of minimizing unused internal volume in such components. In this setup the filter dryer is placed in the liquid line after the condenser. This section is often preferred by the manufacturers of the filter dryers, as it yields the highest effectiveness. However, due to the highest density of the refrigerant in this section, the filter dryer houses a significant amount of the system charge. It should be noted that the internal volume of the filter dryer was only estimated from the manufacturer's drawings, and the entire volume was assumed to be available for refrigerant occupancy. This represents a conservative assumption, as in reality, part of the volume is occupied by the desiccant core and internal structures, and the actual refrigerant mass contained is likely lower.

3.3. Identification of the limiting operating point and maximum charge

To link the component-wise charge predictions to the 150 g releasable-charge limit, parametric charge sweeps were performed for three representative operating points:

- B0/W35 @ 120 Hz (nominal heating at full power),
- B−15/W70 @ 80 Hz (domestic hot water generation), and
- B5/W24 @ 20 Hz (low-load heating).

As an example, the notation B0/W35 @ 120 Hz refers to an operating condition with a brine (source) inlet temperature of 0 °C, a water (sink) outlet temperature of 35 °C, and a compressor speed of 120 Hz. For each operating point, the total refrigerant charge was varied, while the boundary conditions (brine inlet and water outlet temperatures, compressor speed) and control targets (superheat) were kept constant. For every converged simulation, the separated-flow model with the Premoli slip correlation was used to determine the refrigerant mass in each component (as it is most conservative), with particular focus on the condenser, which was previously identified as the component with the largest single charge.

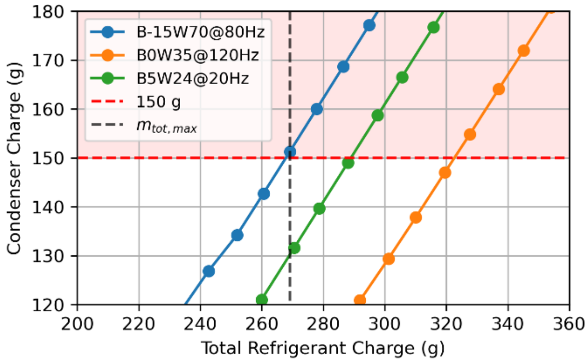

Figure 4: Condenser refrigerant charge as a function of total charge for the three representative operating points. The horizontal line marks the 150 g component limit. The intersection with each curve defines the maximum admissible total charge for that operating point $m_{tot,max,k}$. The lowest value, here occurring at B−15/W70 @ 80 Hz, determines the global maximum filling $m_{tot,max}$ = 269 g that keeps the condenser charge below 150 g under the three conditions presented.

Figure 4 shows that the condenser charge increases almost linearly with total charge for all three operating points. Among the considered conditions, B−15/W70 @ 80 Hz yields the highest mass of refrigerant in the condenser for a given total charge. Consequently, it reaches the 150 g limit at the lowest total charge, making it the most restrictive operating point from a releasable-charge perspective. The global maximum filling determines therefore to $m_{tot,max}$ = 269 g, that keeps the condenser charge below 150 g for the three conditions presented. Therefore, both B0/W35 @ 120 Hz and B5/W24 @ 20 Hz remain safely below 150 g at this total charge level, leaving additional margin. It should be noted that changes in system settings, for example increasing the superheat or imposing restrictions on the compressor speed specifically for the limiting point B−15/W70 @ 80 Hz, could reduce the condenser charge at that operating condition. Such adjustments would relax the constraint and potentially allow a higher total permissible system charge. In summary, strict compliance with the maximum permissible refrigerant charge derived here is essential. Refrigerant circuits of this size are usually charged and sealed using automated equipment during production, ensuring a high level of accuracy. Refilling in the field, on the other hand, is most likely the result of damage to the unit. Due to the unit's compact size, replacing the entire refrigerant circuit or module might be a more practical option than carrying out repairs on site. This would also remove the risk of technicians overcharging the system. Where this is unavoidable, dedicated solutions such as prefilled cartridges with a defined maximum charge are required.

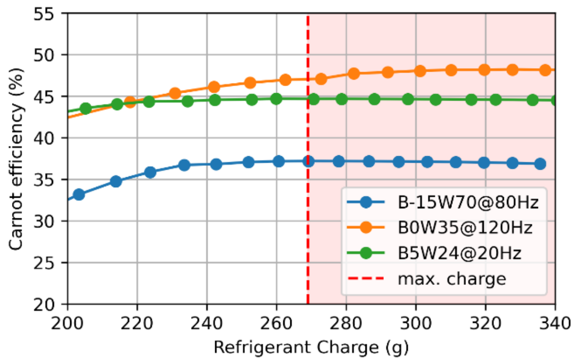

Figure 5: Carnot efficiency versus total system charge for the three representative operating points. The domestic hot water generation (B-15/W70 @ 80 Hz) and low-load heating (B5/W24 @ 20 Hz) points reach their maximum efficiency within the tested charge range, whereas the nominal heating point (B0/W35 @ 120 Hz) would benefit from a higher charge.

Figure 5 illustrates the Carnot efficiency of the heat pump for the three representative operating points, nominal heating (B0/W35 @ 120 Hz), low-load heating (B5/W24 @ 20 Hz), and domestic hot water generation (B-15/W70 @ 80 Hz), as a function of the total system charge. The diagram highlights that the efficiency behavior with increasing refrigerant mass varies distinctly among operating conditions. For the domestic hot water generation (B-15/W70 @ 80 Hz) and low-load heating (B5/W24 @ 20 Hz) points, the Carnot efficiency reaches a maximum within the maximum allowed system charge. In contrast, the nominal heating point (B0/W35 @ 120 Hz) shows a steady rise of the Carnot efficiency with charge, suggesting that higher filling amounts could still enhance performance by improving heat exchanger utilization and increasing the compressor efficiency due to a more favorable pressure ratio.

Conclusions

In this work a one-dimensional simulation model was developed to predict the component-wise refrigerant distribution in a residential propane (R290) heat pump. The model extends beyond state-of-the-art models that use the homogeneous equilibrium model by implementing separated-flow formulations that account for phase slip and by including the solubility of propane in the compressor oil. This combined approach enables a physically consistent estimation of both the liquid and vapor charges, improving the accuracy of total and component-wise charge predictions across various operating conditions.

The comparison of different slip-ratio correlations demonstrated a strong influence on the predicted total refrigerant mass. All separated-flow models yielded higher charge estimates than HEM, confirming that neglecting phase-velocity differences leads to an underestimation of the required refrigerant charge. Among the implemented models, the Premoli correlation provided the most conservative results, predicting the highest total charge. This trend agrees with previous studies highlighting the sensitivity of void-fraction predictions - and thus refrigerant charge - to the applied slip formulation.

For all simulated operating points, the largest share of refrigerant was consistently located in the condenser. This finding corresponds to the higher refrigerant density on the high-pressure side and matches experimental data reported in literature. Consequently, the condenser represents the most critical component for compliance with safety-related charge limits. The model allows direct identification of the operating condition in which refrigerant accumulation in the condenser becomes limiting for the overall system charge.

Through parametric charge sweeps, the domestic-hot-water operating point (B-15/W70 @ 80 Hz) was identified as the most restrictive point, defining a maximum permissible system charge of approximately 269 g to ensure that no single component exceeds 150 g. This value sets an upper bound for safe operation of the investigated configuration.

Future work will focus on three main directions:

- Adaption of limiting point - adjustment of system settings (e.g. superheat, compressor speed restrictions) to reduce condenser charge at the most restrictive operating point and thereby enable a higher allowable total system charge, including an investigation on the sensitivity of subcooling to the filled charge.
- Dynamic circuit control - implementation of a valve logic to isolate circuit at a leak event, including evaluation of efficiency losses due to additional pressure drops.
- Experimental validation - verification of the simulated charge distribution through experimental measurements on an operating prototype.
- Safety integration - coupling of the 1D model with detailed 3D CFD dispersion simulations to assess leakage and ventilation behavior for indoor installation.

Acknowledgements

This work was funded by the Austrian Research Promotion Agency (FFG) under grant no. 54638052.

References

[1] International Energy Agency (IEA), *The Future of Heat Pumps*. OECD, 2022. Accessed: Nov. 06, 2025. [Online]. Available: https://www.oecd.org/en/publications/the-future-of-heat-pumps_2bd71107-en.html

[2] European Parliament and Council of the European Union, “Regulation (EU) 2024/573 of the European Parliament and of the Council of 7 February 2024 on fluorinated greenhouse gases, and repealing Regulation (EU) No 517/2014.” Official Journal of the European Union, Feb. 2024. [Online]. Available: https://eur-lex.europa.eu/legal-content/EN/TXT/?uri=CELEX%3A32024R0573

[3] United Nations, “Amendment to the Montreal Protocol on Substances that Deplete the Ozone Layer (Kigali Amendment).” United Nations, Oct. 15, 2016. [Online]. Available: https://treaties.un.org/doc/Publication/CN/2016/CN.872.2016-Eng.pdf

[4] European Committee for Standardization (CEN), “EN 378-1:2021 — Refrigerating systems and heat pumps — Safety and environmental requirements — Part 1: Basic requirements, definitions, classification and selection criteria.” Vienna, Austria, Jun. 2021. [Online]. Available: https://www.austrian-standards.at/de/shop/din-en-378-1-2021-06~p2583565

[5] European Committee for Electrotechnical Standardization (CENELEC), “OVE/ÖNORM EN 60335-2-40:2014 — Household and similar electrical appliances — Safety — Part 2-40: Particular requirements for electrical heat pumps, air-conditioners and dehumidifiers.” Vienna, Austria, Feb. 2014. [Online]. Available: https://www.austrian-standards.at/de/shop/ove-onorm-en-60335-2-40-2014-02-01~p2426852

[6] J. Winkler, J. Killion, S. Garimella, and B. M. Fronk, “Void fractions for condensing refrigerant flow in small channels: Part I literature review,” *Int. J. Refrig.*, vol. 35, no. 2, pp. 219–245, Mar. 2012, doi: 10.1016/j.ijrefrig.2011.09.013.

[7] L. Schnabel, T. Methler, A. H. Hassan, C. Dankwerth, and J. M. G. Maciá, “Design and Analysis of Charge-Reduced Refrigerant Cycles Using R290,” *Chem. Ing. Tech.*, vol. 95, no. 3, pp. 353–362, 2023, doi: 10.1002/cite.202200150.

[8] L. Sánchez-Moreno-Giner, T. Methler, F. Barceló-Ruescas, and J. Gonzálvez-Maciá, “Refrigerant charge distribution in brine-to-water heat pump using R290 as refrigerant,” *Int. J. Refrig.*, vol. 145, pp. 158–167, Jan. 2023, doi: 10.1016/j.ijrefrig.2022.10.013.

[9] TLK-Thermo GmbH, “TIL Suite - Simulates thermal systems,” Braunschweig, 2022. [Online]. Available: https://tlk-thermo.com/index.php/en/software/til-suite

[10] FUCHS Lubricants, “RENISO Refrigeration Oils — Product Brochure.” 2023. [Online]. Available: https://www.fuchs.com/de/de/produkte/download-center/download/file/232687-RENISO-Kaltemaschinenole-Broschure/

[11] S. M. Zivi, “Estimation of steady-state steam void-fraction by means of the principle of minimum entropy production,” *ASME J. Heat Transf.*, vol. 86, pp. 247–251, 1964, doi: 10.1115/1.3687093.

[12] A. Premoli, D. Francesco, and A. Prina, "An Empirical Correlation for Evaluating Two-Phase Mixture Density under Adiabatic Conditions," in *Proceedings of the European Two-Phase Flow Group Meeting*, Milan, Italy, 1970.
[13] M. I. Ali, M. Sadatomi, and M. Kawaji, "Adiabatic two-phase flow in narrow channels between two flat plates," *Can. J. Chem. Eng.*, vol. 71, no. 5, pp. 657–666, Oct. 1993, doi: 10.1002/cjce.5450710502.
[14] L. Schnabel, K. Morawietz, T. Methler, T. Oltersdorf, H. Fugmann, and C. Dankwerth, "LC150 – Entwicklung eines kältemittelreduzierten Wärmepumpenmoduls mit Propan," Fraunhofer-Institut für Solare Energiesysteme ISE, Freiburg, Germany, Abschlussbericht Fkz: 03EN4001A, 2023. [Online]. Available: https://edocs.tib.eu/files/e01fb24/1887994033.pdf